20th International Congress on Modelling and Simulation, Adelaide, Australia, 1–6 December 2013
www.mssanz.org.au/modsim2013

Error characterization of microwave satellite soil moisture data sets using Fourier analysis

Chun-Hsu Su[a], Dongryeol Ryu[a], Andrew W. Western[a], Wade T. Crow[b], Wolfgang Wagner[c]

[a] *Department of Infrastructure Engineering, The University of Melbourne, Victoria, Australia*
[b] *Hydrology and Remote Sensing Laboratory, USDA Agricultural Research Service, Maryland, USA*
[c] *Department of Geodesy and Geoinformation, Vienna University of Technology, Vienna, Austria*
Email: csu@unimelb.edu.au

Abstract: Soil moisture is a key geophysical variable in hydrological and meteorological processes. Accurate and current observations of soil moisture over meso to global scales used as inputs to hydrological, weather and climate modelling will benefit the predictability and understanding of these processes. At present, satellite platforms are active in mapping global surface soil moisture jointly at sub-daily intervals and mesoscale resolutions. However to correctly interpret observed variations and assimilate them in hydrological and weather models, the error structures of the retrieved soil moisture data need to be better understood and characterised.

In this paper we investigate the utility of a recently proposed method to quantify the variance of stochastic noise in passive and active satellite soil moisture products. While it is typical to analyse the difference between satellite retrievals and ground truth in the *time* domain, this method is based on quantifying the differences between retrieved soil moisture and a standard water-balance equation in the conjugate *Fourier* domain. The method, which referred to as Spectral Fitting (SF), is applied to estimate the errors in passive and active retrievals over Australia (10-44^o South, 112-154^o East). In particular we consider the AMSR-E (Advanced Microwave Scanning Radiometer – Earth Observing System) LPRM (Land Parameter Retrieval Method), CATDS (Centre Aval de Traitement des Données SMOS) SMOS (Soil Salinity and Ocean Salinity), and TU-WIEN (Vienna University of Technology) ASCAT (Advanced Scatterometer) soil moisture products. The results are compared against the errors estimated using the standard method of triple collocation (TC) with AMSR-E, SMOS and ASCAT as the data triplet.

Our analyses show that the SF method is able to recover similar and reasonable error maps that reflect sensitivity of retrieval errors to land surface and climate characteristics over Australia. As expected, more vegetated and wetter areas are usually associated with higher errors. Additionally for SMOS and ASCAT, the dry cooler desert areas of southern Australia also show higher errors, in contrast to lower errors over the hotter dry desert of central Australia. The reverse is the case for AMSR-E. These patterns are also reflected in the spatial error maps of TC analysis and the direct comparisons of SF and TC estimates show moderate-to-good correlations: 0.64 for AMSR-E, 0.68 for SMOS, and 0.68 for ASCAT. However the SF yields lower estimates than TC at the high end of the range. On one hand, this is perhaps expected given rationale of the SF method to estimate only the stochastic/high-frequency components of the total errors. On the other hand, the simple error model and implementation of TC with non-coincident overpass times can also over-estimate the errors.

This work therefore presents an additional perspective on satellite soil moisture observation errors (in the Fourier domain) that may complement other error estimation approaches (in the time domain), thereby improving our understanding of the sources and types of errors.

Keywords: *Soil moisture, Satellite remote sensing, error characterization, Fourier analysis, triple collocation*

1. INTRODUCTION

Soil moisture (SM) is an essential geophysical variable in hydro-meteorological and climate studies. To achieve accurate modeling at large scales, frequent mesoscale observations of terrestrial SM are necessary due to high spatiotemporal heterogeneity. Satellite remote sensing provides this capability and, at present, several satellite platforms are active in mapping global surface SM on a (near) daily basis. In order to use these observations with confidence, characterization of their errors is critical. For instance, when calibrating or rescaling one data set against the other, it is important to know the errors because linear regression leads to under-estimation of the signal. Also, optimal data assimilation methods require accurate error estimates to assign correct weights to observational data and model prediction. Error characterization can also provide further insights into retrieval sensitivities to land surface characteristics.

Currently there are two methods for estimating the errors in satellite SM data without relying on ground truth. The first method is triple collocation (TC) (Stoffelen, 1998), which uses the covariances between three independent estimates of SM related by an affine model to solve for their error variances (Scipal et al., 2008). To achieve statistically-convergent estimates, large number of linearly-related coincident observations with independent error structures from three sensors are required (Zwieback et al., 2012). This can however be difficult to realise in practice. The second method implements propagation of input errors using Gaussian error propagation (Naeimi et al., 2009) or partial derivatives of radiative transfer model for passive retrievals (Parinussa et al. 2011). These methods assume *a priori* knowledge of input and model structural errors, although they do enable time-dependent estimations of the retrieval errors.

Within this context, we consider an alternative approach proposed in Su et al. (2013a) to the problem –we measure the difference between the empirical power spectra of the SM observations and the spectrum of a water balance equation in the Fourier domain to estimate the variance of stochastic noise (possibly a subset of the total error) in the satellite data. We apply this method to three satellite SM products: Advanced Microwave Scanning Radiometer – Earth Observing System (AMSR-E), Soil Moisture and Ocean Salinity (SMOS) mission, and Advanced Scatterometer (ASCAT) of MetOp-A satellite. TC is also implemented for comparisons. Spatial error estimates are made over Australia (10-44^{o} South, 112-154^{o} East). Possible associations with vegetation and rainfall distributions are also investigated.

2. DATA SETS

The AMSR-E sensor aboard the Aqua satellite provided C and X-band radiance observations used to retrieve surface SM at 1-5 mm surface depth during the period 6/2002 to 10/2011. It provided daily scans of Australia during the mid-day ascending (1.30pm local time) and night time descending (1.30am) orbits. Most retrieval approaches implemented different forms of forward model inversion of the radiative transfer model of canopy-masked soil surface to convert measured brightness temperatures to SM. The Land Parameter Retrieval Model (LPRM) approach (Owe et al., 2008), used AMSR-E's dual-polarization observations at C/X-bands to estimate the vegetation optical depth (VOD) and the dielectric constant, and the 37 GHz channel to estimate the land surface temperature. Here we use the version 5, Level 3 gridded, combined C and X-band SM data set provided in units of volumetric SM on a regular 0.25^{o} latitude and longitude grid.

The SMOS satellite was launched in 11/2009 and is dedicated to SM retrieval at ~5 cm depth using observations at L-band. The ascending overpass over Australia is around 6am local time, and descending pass at 6pm. It has a single observation frequency, but uses observations at multiple incident angles. The standard SMOS algorithm is based on the L-MEB (L-band Microwave Emission of the Biosphere) model and, like the LPRM, it adopts a forward modeling approach to solve for SM and VOD (Wigneron et al., 2007). However, the algorithm has an additional degree of freedom to accommodate different soil types and land covers. We use the Reprocessed (version RE01) SM data set (1/2010 – 3/2012) provided by Centre Aval de Traitement des Données (Jacquette et al., 2010). Their multi-orbit retrieval algorithm extends the standard algorithm to provide better estimations at revisited locations, take auto-correlation of VOD into account, increase SMOS retrieval coverage, and resample swath data on an Equal-Area Scalable Earth (EASE) grid.

The ASCAT sensor onboard the MetOp-A satellite transmits and measures electromagnetic waves in C-band at multiple incidence angles. These measurements over Australia are obtained about twice a day, at ~9am and 9pm. The backscatter is sensitive to the SM content of the scattering land surface and by using a time-series based change-detection algorithm (Wagner et al., 1999), the SM changes can be measured in relative terms, thus become less susceptible to the adverse influence of vegetation cover and surface roughness on retrievals. The ASCAT data set (1/2007 – 12/2012) is defined over a sinusoidal grid with ~12.5 km spacing, and was produced using Water Retrieval Package Version 5.4 (Naeimi et al., 2009).

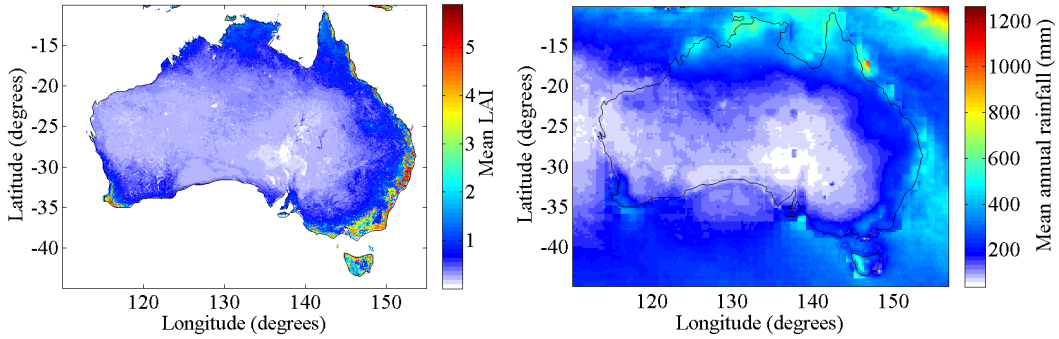

Figure 1. (a) Vegetation characteristics across Australia using MODIS-retrieved leaf-area index (LAI). (b) Mean annual rainfall distribution based on re-processed TRMM 3B42 data set.

Satellite SM products are expected to have declining retrieval accuracy with increasing vegetation. One effect is the reduced signal-to-noise ratio of the observed surface emission against background contributions due to signal attenuation by vegetation, and the other is related to the ability of the retrieval methods to estimate and correct for this attenuation. We explore this possibility by comparing the derived error map with the leaf-area index (LAI) retrieved by MODIS (Moderate Resolution Imaging Spectroradiometer) on Terra/Aqua satellites. The 2001-2010 LAI estimates of ~1x1 km^2 resolution produced by CSIRO (Commonwealth Scientific and Industrial Research Organization) (Paget & King, 2008) are used to provide daily average LAI across Australia, as shown in Figure 1a. The regional climatology may also have associations with errors in satellite retrievals. We use re-processed TRMM (Tropical Rainfall Measuring Mission) 3B42 (Huffman et al., 2007) Version 7 data over the period 2001-2010. The data is available at 3-hourly intervals on a regular 0.25^o grid and is aggregated to produce mean annual rainfall map in Figure 1b.

3. METHODOLOGY

3.1. Model fitting in Fourier domain

Here we describe the method used to estimate the respective stochastic errors in the three satellite products. The method, which we refer to as Spectral Fitting (SF), is a stand-alone procedure that measures the difference between observed SM and expected SM dynamics stipulated by a water balance equation in the Fourier domain. In particular, the dynamics of SM at any spatial scale (point-scale or coarse scale, (Salvucci et al., 2001)) is governed by the equation,

$$\frac{d\theta(t)}{dt} = \frac{p(t) - l(t)}{\mu} \tag{1}$$

where θ is the topsoil water content in the surface layer, p is the throughfall precipitation rate, l is the total loss rate from the layer due to surface runoff, evaporative loss and drainage, and μ is the layer thickness. Invoking a linear approximation that the drainage is proportional to the amount of soil water such that $l(t)/\mu = \eta\theta(t)$ and a Poisson model of precipitation arrival times, the differential equation can be solved in the Fourier domain to yield a solution for the power spectrum of the SM (Su et al. 2013a),

$$\left|\Theta(\omega)\right|^2 = \frac{P^2}{\eta^2 + \omega^2}, \tag{2}$$

for $\omega>0$, where $\Theta(\omega)$ and $P(\omega)=P(\omega>0)$ are the Fourier transforms (FT) of $\theta(t)$ and $p(t)/\mu$ respectively, η is the effective loss rate, and $\omega = 2\pi/T$ is the angular frequency of a spectral component with period T. The water balance equation therefore predicts that the small-time scale SM dynamics (in the large ω regime) mimic Brownian motion and have a brown-like spectrum that scales as ω^{-2} in the high-frequency regime.

Assuming an additive Gaussian white-noise error with spectral amplitude E and error variance σ_e^2, the FT of erroneous satellite data is,

$$\Theta_{sat}(\omega) = \Theta(\omega) + E, \tag{3}$$

so that its power spectrum becomes,

$$|\Theta_{sat}(\omega)|^2 = \frac{(P+\eta E)^2 + \omega^2 E^2}{\eta^2 + \omega^2}. \quad (4)$$

In the final step, we recast the power spectrum as power spectral density (PSD) (i.e., equivalent up to a multiplicative constant) and note that E in the Fourier domain and σ_e^2 in the time domain are related by,

$$E^2 = \sigma_e^2 \Delta t, \quad (5)$$

for a sampling interval of Δt. Eqs. 4 and 5 therefore form the basis for estimating the amount of stochastic noise in the satellite products. In sum, given a satellite SM time series input, we estimate its PSD using fast Fourier transform and by fitting the model in Eq. 4 to the PSD, we arrive at an estimate of E (together with other model parameters P and η) and the error variance via Eq. 5. Su et al. (2013a) showed that half a year of data is sufficient for reliable estimation of the PSD in the high-frequency regime.

3.2. Triple collocation

Triple collocation (TC) is now a widely-used method for estimating errors in hydrometeorological and oceanographical data sets. Given three spatially and temporally co-located measurements of the same target variable f, TC adopts an affine model to relate the data sets,

$$X = \langle X \rangle + f + \varepsilon_x, \quad Y = \langle Y \rangle + \alpha f + \varepsilon_y, \quad Z = \langle Z \rangle + \beta f + \varepsilon_y, \quad (6)$$

where X acts as the reference, $\langle \circ \rangle$ denotes the expectation value of the given parameter, $\varepsilon_x, \varepsilon_y, \varepsilon_z$ are zero-mean Gaussian random errors orthogonal (independent) to one another, and α and β are multiplicative biases. Differences in means act as additive biases between the data sets. The statistical relations between the three data sets provide sufficient constraints to determine their error variances simultaneously. Specifically with the changes of variables $X \to X - \langle X \rangle$, $Y \to Y - \langle Y \rangle$, and $Z \to Z - \langle Z \rangle$, it can be shown that,

$$\langle \varepsilon_x{}^2 \rangle = \langle X^2 \rangle - \frac{\langle XY \rangle \langle XZ \rangle}{\langle YZ \rangle}, \quad \langle \varepsilon_y{}^2 \rangle = \langle Y^2 \rangle - \frac{\langle XY \rangle \langle YZ \rangle}{\langle XZ \rangle}, \quad \langle \varepsilon_z{}^2 \rangle = \langle Z^2 \rangle - \frac{\langle XZ \rangle \langle YZ \rangle}{\langle XY \rangle}, \quad (7)$$

In some cases where there is no exact solution, approximate solutions are determined by solving Eq. 7 using constrained nonlinear minimization.

We use the TC method with the AMSR-E (X), SMOS (Y) and ASCAT (Z) data sets to determine their error variances. Then, given that the SF model is compatible with these error characteristics, the TC-estimated error variance are directly compared with those estimated with the SF method. The satellite observations are made at different times. In order to apply the TC technique, we consider the triplet of overpass times 6am (SMOS), ~9am (ASCAT), 1.30pm (AMSR-E) to be coincident in time. The next triplet is 6pm (SMOS), ~9pm (ASCAT), and 1.30am (AMSR-E). It is important to realize that instances where there was rainfall during intermediate periods of satellite overpasses could artificially inflate the estimated errors. Therefore the TRMM rainfall data was used to identify and remove these instances from the analysis. Finally, we note that errors of day and night-time retrievals are typically different due to variable thermal conditions; but since both data are used jointly in the SF and TC analyses, their error estimates will represent some average of the two and are directly comparable.

3.3. Data pre-processing

The three SM products are gridded differently and have different spatial resolutions. To allow direct comparisons of the three products, we followed the approach described in Su et al. (2013b) to resample SMOS and ASCAT data sets to match the working spatial 0.25° grid of AMSR-E. For SMOS we use area-weighted averages based on the overlap between satellite pixels. For ASCAT, there are several retrieval points uniformly distributed within a 0.25° pixel. To avoid artificial biases introduced by upscaling, individual points are first converted to volumetric units using ancillary soil porosity data then averaged to an areal estimate. All data points identified with error flags were eliminated. In particular, for ASCAT, the data were masked when quality flag SSF > 1, the advisory on water fraction was >50%, the snow advisory was > 0, or the frozen soil advisory was > 0. For AMSR-E and SMOS, poor-quality retrievals with quality flags SSF and DQX < 0 were eliminated. These re-processing steps led to the baseline data sets for SF and TC. Spatial resampling using equal-weighted averaging was also performed on the LAI data.

Following Draper et al. (2013), we apply TC on SM anomalies, which are defined by deviations from the seasonal cycle and are calculated using a W=30-day moving window. As there are many missing values in

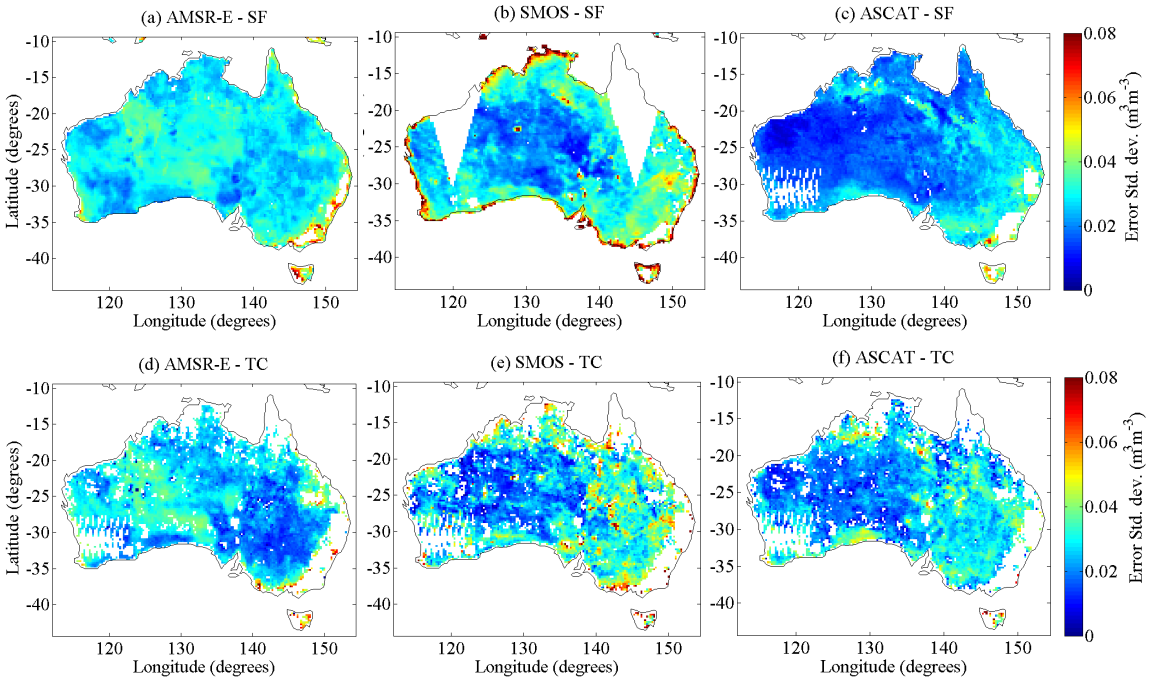

Figure 2. Error maps over Australia for different satellite products, estimated using SF (a-c) and TC (d-f). Note that the range of the colour map is truncated at 0.08 m^3m^{-3}.

the data sets due to overpass alignment and swath width limitations, we retain the anomaly estimates calculated with windows containing a minimum 35% of valid data. Furthermore calculations were performed at locations with ≥100 triplets.

To perform SF, we require regularly sampled data in time. To obtain a suitable timeseries segment for error analysis, the following steps were taken: (1) For each retrieval location or grid cell, the longest continuous timeseries segment (containing at most 3 days or equivalently 6 consecutive missing values) was selected. Since we assume stationary stochastic noise, we do not limit the specific time frames from which the segments are selected. (2) Segments of length shorter than 9 months are omitted. Segments with more than 65% missing values are also omitted. The 65% threshold was chosen for ASCAT, since AMSR-E and SMOS typically contains 50–60%. (3) A one-dimensional gap-filling algorithm based on discrete cosine transform (Wang et al., 2012) was used to infill the missing values in the selected segments.

4. RESULTS AND DISCUSSION

Figure 2 shows the error estimates for the three satellite products estimated by SF and TC over Australia. Note that for SMOS, the gaps in Figure 2b are regions with small samples (< 9 months). Visual inspections of the spatial structure of the SF error maps show similarities between the products. The more vegetated and wetter areas (see Figure 1a and b) are usually associated with higher errors. The retrievals over the transitional regions from tropical savannah (Köppen Aw, Peel et al., 2007) to hot arid steppe regions (BSh) in the northern parts also show increased errors. For SMOS and ASCAT, the dry cooler desert areas (BWk) of southern Australia also register larger errors, although these regions experience small SM variability. By contrast, over the hot dry desert in the central regions, SF identified smaller errors in SMOS and ASCAT, but larger errors in AMSR-E. In the eastern areas, the products, especially SMOS and ASCAT, show markedly larger errors in the Murray Darling Basin (BSh, Cfa). Comparing the SF and TC maps, one can discern several similarities. Many features identified in SF maps above are also reflected in these maps.

There are also some notable differences. In particular, TC reveals smaller-scale error structures that reflect the complexity of associated land characteristics with a mix of vegetation and river systems. There is also greater spatial heterogeneity in errors in central Australia. Figure 3 provides quantitative comparisons of SF and TC estimates in terms of Pearson's correlation, R, where the 95% confidence interval is calculated using Fisher's transform. For all 3 products, there exists significant association (R=0.64–0.68) between SF and TC estimates. But it is obvious that SF generally yields lower estimates at the high-error limit. The possible reasons for these differences are as follows.

Recall that the basis of SF is to distinguish stochastic errors that become apparent in the high-frequency regime. One possible explanation is that, contrary to the white noise assumption in the SF, the stochastic

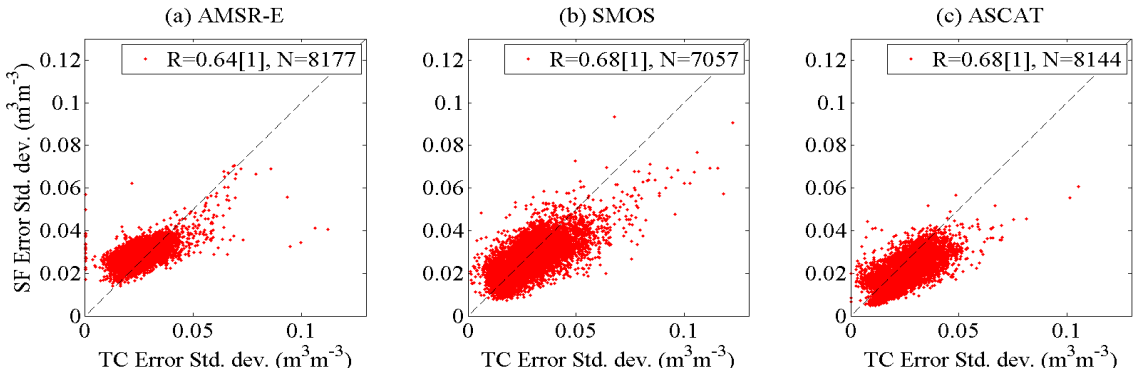

Figure 3. Scatterplots comparing the error estimates from the two methods. *R* is the Pearson's correlation with 95% CI in square brackets (e.g., 0.64[1] has a CI of 0.01), and *N* identifies the number of pixels.

Table 1. Summary of correlations between a range of variables (mean SM, leaf-area index (LAI), and mean annual rainfall) and error estimates using different methods for different satellite products. The square brackets indicate the 95% CI.

		Correlation with error std. dev.		
Products	Estimator	Mean SM	LAI	Rainfall
AMSR-E	SF	0.36[2]	0.51[1]	0.24[2]
	TC	0.17[2]	0.43[1]	0.29[2]
SMOS	SF	0.82[1]	0.61[1]	0.45[2]
	TC	0.73[1]	0.46[1]	0.30[2]
ASCAT	SF	0.64[1]	0.48[2]	0.25[2]
	TC	0.42[2]	0.16[2]	0.06[2]

noise may be autoregressive in nature. However the autocorrelation in the noise should be weak for AMSR-E retrievals because every retrieval is based on instantaneous observations and the LPRM does not rely on ancillary data. SMOS' reliance on ancillary sources of land surface temperature may render it more susceptible to autoregressive errors. Another issue is that additional spectral features at high frequencies exist. Su et al. (2013a) found resonance peaks in AMSR-E and SMOS and non-uniform spectral distribution in ASCAT, and they can affect the error estimation. This consideration led to the choice of using absolute deviations as the cost function for model fitting; however, the presence of these spectral features can still lead to higher estimates. Nevertheless these considerations suggest the tendency of SF to over-estimate the variance of stochastic errors, whilst the results in Figure 3 suggest the contrary. It is more likely that gap-filling algorithm adds in smooth segments to the data or the difference may be attributed to TC analysis.

The simple error model of TC can lead to larger error estimates. The additional components observed in the satellite products in the Fourier domain suggest that the systematic differences between the three data sets are not merely multiplicative and additive biases. These additional spectral features are product-specific signals (e.g., due to representation differences or biased sampling) that can artificially inflate the TC-based error estimates. Additionally, specific practices of data pre-processing such as removing seasonality (Draper et al. 2013) and the choice of data triplets (e.g., use of model SM) can also change the error characteristics. In particular, while the combination of two passive and one active retrievals has also been considered previously (e.g., Leroux et al., 2011), the use of similar radiative transfer (τ-ω) model for retrieving SM from AMSR-E and SMOS may lead to cross correlations in their errors, undermining the mutually independent error assumption – this dependency will be investigated in future work.

In the final but preliminary analysis (Table 1), we explore possible associations between the spatial structures of the errors and several other variables, namely the regional soil wetness (or the temporal mean moisture), vegetation cover indicated by LAI and the rainfall distribution. First, we find that mean soil wetness is associated with higher errors in SMOS, (R=0.82 (SF) and 0.73 (TC)). It is also a reasonable predictor for the SF-based error map for ASCAT. Despite visual similarities between the LAI, rainfall and error maps, we observed that static vegetation and rainfall characteristics are generally weak indicators of error levels. Future studies will consider the topographical and variability of the land surface to better understand the revealed error structures.

5. CONCLUSIONS

This study has compared two error estimators, TC and SF, applied to three remotely-sensed SM data sets over Australia. Despite fundamental differences in concepts and implementations, the two methods produce

structurally similar and reasonable error maps that allow one to relate the retrieval errors to land surface and climate characteristics. For the three satellite products, we find fair-to-good correlations between the SF and TC error estimates. However in absolute terms, the SF yields lower estimates in the large-error limit. While SF may under-estimate the overall errors by only estimating its stochastic components or due to the gap-filling, the simplicity of the error model and data pre-processing for TC also warrant careful deliberation. By comparing the different error estimation approaches (including error propagation), we can better understand the nature of the differences between different satellite products and attribute the sources of their errors, and examining their spectral characteristics may provide these further insights.

ACKNOWLEDGMENTS

We thank Kaighin McColl, Robert Parinussa, Clara Draper for valuable discussions. The SMOS level 3 data were obtained from the "Centre Aval de Traitement des Données SMOS" operated for the "Centre National d'Etudes Spatiales" (CNES) by IFREMER (Brest, France). ASCAT level 3 data were produced by the Vienna University of Technology within the framework of EUMETSAT's Satellite Application Facility on Support of Operational Hydrology and Water Management from MetOp-A observations. This research was conducted with financial support from the Australian Research Council (ARC Linkage Project No. LP110200520).

REFERENCES

Draper, C. S., Reichle, R. R., de Jeu, R. A., Naeimi, V., Parinussa, R. M., and Wagner, W., Estimating root mean square errors in remotely sensed soil moisture over continental scale domains. *Remote Sensing of Environment*, in press.

Huffman, G. J., et al. (2007). The TRMM Multisatellite Precipitation Analysis (TMPA): Quasi-Global, Multiyear, Combined-Sensor Precipitation Estimates at Fine Scales. *Journal of Hydrometeorology*, 8, 38-55.

Jacquette, E., et al. (2010). SMOS CATDS level 3 global products over land, *Proceeding SPIE7824. Remote Sensing for Agriculture, Ecosystems, and Hydrology, XII*, 78240K.

Leroux, D. J., Kerr, Y. H., Richaume, P., and Berthelot, B. (2011). Estimating SMOS error structure using triple collocation. *Proceeding of IEEE International Geoscience and Remote Sensing Symposium (IGARSS) 2011*, 24-27.

Naeimi, V., Scipal, K., Bartalis, Z., Hasenauer, S., and Wagner, W. (2009). An improved soil moisture retrieval algorithm for ERS and METOP scatterometer observations. *IEEE Transanctions on Geoscience and Remote Sensing*, 47 , 1999–2013.

Owe, M., de Jeu, R., and Holmes, T. (2008). Multisensor historical climatology of satellite-derived global land surface moisture. *Journal of Geophysical Research*, 113, F01002.

Paget, M. J. and King, E. A. (2008). MODIS land data sets for the Australian region. CSIRO Marine and Atmospheric Research Internal Report 004, Canberra, Australia.

Parinussa, R., Meesters, A., Liu, Y., Dorigo, W., Wagner, W., and de Jeu, R. (2011). Error estimates for near-real-time satellite soil moisture as derived from the Land Parameter Retrieval Model. *IEEE Journal of Selected Topics in Applied Earth Observations and Remote Sensing*, 8, 779–783.

Peel, M.C., Finlayson, B.L., and McMahon, T.A., 2007. Updated world map of the Köppen-Geiger climate classification. *Hydrological and Earth System Science*, 11, 1633-1644.

Salvucci, G. D. (2001). Estimating the moisture dependence of root zone water loss using conditionally averaged precipitation. *Water Resources Research*, 37, 1357-1365.

Scipal, K., Holmes, T., de Jeu, R., Naeimi, V., and Wagner, W. (2008). A possible solution for the problem of estimating the error structure of global soil moisture data sets. *Geophysical Research Letters*, 35, L24403.

Stoffelen, A. (1998). Towards the true near-surface wind speed: Error modelling and calibration using triple collocation. *Journal of Geophysical Research*, 103, 7755-7766.

Su, C.-H., Ryu, D., Western, A. W., and Wagner, W. (2013a). De-noising of passive and active microwave satellite soil moisture time series. *Geophysical Research Letters*, 40, 3624-3630

Su, C.-H., Ryu, D., Young, R. I., Western, A. W., and Wagner, W. (2013b). Inter-comparison of microwave satellite soil moisture retrievals over the Murrumbidgee Basin, southeast Australia. *Remote Sensing of Environment*, 134, 1-11.

Wagner, W., Lemoine, G., and Rott, H. (1999). A method for estimating soil moisture from ERS scatterometer and soil data, *Remote Sensing of Environment*, 70, 191-207.

Wang, G., Garcia, D., Liu, Y., de Jeu, R., and Dolman, J. (2012). A three-dimensional gap filling method for large geophysical datasets: Application to global satellite soil moisture observations. *Environmental Modelling & Software*, 30, 139-142.

Wigneron, J.-P., et al. (2007). L-band Microwave Emission of the Biosphere (L-MEB) model: Description and calibration against experimental data sets over crop fields. *Remote Sensing of Environment*,107, 639-655.

Zwieback, S., Scipal, K., Dorigo, W., and Wagner, W., (2012). Structural and statistical properties of the collocation technique for error characterisation. *Nonlinear processes in Geophysics*, 19, 69-80.